Andreev conductance of chaotic and integrable quantum dots

A. A. Clerk, P. W. Brouwer, and V. Ambegaokar
Laboratory of Atomic and Solid State Physics, Cornell University, Ithaca, New York 14853
(Received 20 April 2000)

We examine the voltage V and magnetic field B dependent Andreev conductance of a chaotic quantum dot coupled via point contacts to a normal metal and a superconductor. In the case where the contact to the superconductor dominates, we find that the conductance is consistent with the dot itself behaving as a superconductor—it appears as though Andreev reflections are occurring locally at the interface between the normal lead and the dot. This is contrasted with the behavior of an integrable dot, where for a similar strong coupling to the superconductor no such effect is seen. The voltage dependence of the Andreev conductance thus provides an extremely pronounced quantum signature of the nature of the dot's classical dynamics. For the chaotic dot, we also study nonmonotonic reentrance effects that occur in both V and B.

I. INTRODUCTION

Though the actual process of Andreev reflection is simple to describe—an electron in a normal metal incident on a superconductor is reflected back as a hole[1]—it serves as the fundamental basis for some of the most striking effects known in mesoscopic physics.[2] In particular, Andreev reflection may be viewed as the phenomenon underlying the proximity effect, in which a superconductor is able to strongly influence the properties of a nearby normal metal. Andreev reflection is also the process responsible for the unique conductance properties of normal-superconducting (NS) junctions, such as the conductance enhancement observed in NS point contacts.

Attention has recently turned to so-called Andreev billiards as ideal systems in which to study the proximity effect.[3–10] Such systems consist of an isolated normal metal region, small enough that electrons remain phase coherent within it (i.e., a quantum dot), coupled weakly through a point contact to a superconducting electrode. Calculations of the density of states in such structures have shown, rather remarkably, that the proximity effect is sensitive to the nature of the classical dynamics—a gap of size $\tilde{\Delta}$ in the spectrum is present in the case of a chaotic billiard, whereas in the integrable case the density of states vanishes linearly at the Fermi energy.[5,7]

In the present work we also focus on the Andreev billiard, but now add a second point contact leading to a normal electrode and investigate the Andreev conductance of the resulting structure. The Andreev conductance is the differential conductance dI/dV at voltages smaller than the superconducting gap in the S electrode, where Andreev reflection at the interface between the normal metal dot and the superconductor is the only current carrying mechanism. Unlike previous studies,[11,12] here we calculate the full voltage (V) and magnetic field (B) dependence of the conductance.

Two questions are of particular interest in this study. First, does the sensitivity of the proximity effect to chaotic versus integrable dynamics, as seen in the density of states, also manifest itself in the Andreev conductance? We find that indeed it does. In the case where the contact to the superconducting electrode is much wider than that to the normal electrode, the V and B dependent conductance of a chaotic dot is consistent with assuming that the dot has itself become superconducting. The conductance is doubled with respect to the normal state, and remains bias independent until eV reaches the induced gap $\tilde{\Delta}$ in the Andreev billiard. This is in sharp contrast to what is found in exact calculations for integrable dots. For both rectangular and circular dot geometries, the conductance drops off linearly with voltage without any plateau near $V=0$. We argue that this difference is ubiquitous for integrable versus chaotic systems.

The second motivation for the present study is the question of reentrance effects—is the behavior of the conductance simply monotonic in V and B? In the case of a diffusive NS junction, it is well known that this is not the case.[13,14] At zero voltage and also at voltages large enough to break electron-hole degeneracy, the conductance of the junction is the same as in the normal state. However, a conductance enhancement does occur at intermediate voltages. We examine reentrance effects in the conductance of chaotic Andreev billiards, both in the case of ballistic contacts and in the case where both point contacts contain opaque tunnel barriers.

The remainder of this paper is organized as follows. In Sec. II, we present our model for the chaotic dot and introduce the technique used to calculate the voltage and field dependent Andreev conductance. In Sec. III, we discuss results in the case where the contact to the superconductor dominates the contact to the normal electrode, and contrast the results for a chaotic billiard with exact quantum mechanical calculations for two integrable systems. In Sec. IV, we discuss reentrance effects. We conclude with a synopsis of our key results in Sec. V.

II. MODEL AND TECHNICAL DETAILS

A. Formulation of the problem

We consider a chaotic quantum dot coupled via point contacts to a normal metal and a superconductor having, respectively, N_N and N_S propagating modes at the Fermi energy E_F (see Fig. 1). We assume that the ergodic time is much shorter

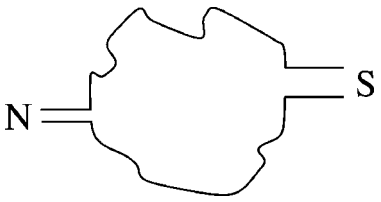

FIG. 1. Schematic drawing of a dot coupled via point contacts to a normal metal and a superconductor.

than other relevant time scales of the dot (i.e., the inverse superconducting gap $\hbar/\Delta$ and the dwell time), so that random matrix theory[15] (RMT) may be used to describe its transport and spectral properties. In RMT, the Hamiltonian of the dot is represented by an $M\times M$ Hermitian matrix H, which, at zero magnetic field, is real symmetric and a member of the Gaussian orthogonal ensemble:

$$P(H)=\exp\left(-\frac{1}{4}M\lambda^{-2}\mathrm{tr}\,H^2\right). \tag{2.1}$$

The matrix size M is sent to infinity at the end of the calculation. The energy scale λ is related to the mean level spacing 2δ by $\lambda=2M\delta/\pi$. More specifically, 2δ is the mean level spacing for particlelike excitations in the absence of coupling to the superconductor; with the superconductor, the relevant excitations are of mixed particle-hole type, and have a level spacing δ for excitation energies much larger than the gap energy.

In the case of a nonzero magnetic field, the Hermitian matrix H is a member of the Pandey-Mehta distribution:[15,16]

$$P(H)\propto\exp-\left(\frac{M(1+\gamma^2)}{4\lambda^2}\times\sum_{i,j=1}^{M}[(\mathrm{Re}\,H_{ij})^2+\gamma^{-2}(\mathrm{Im}\,H_{ij})^2]\right). \tag{2.2}$$

As γ increases from 0 to 1, the distribution evolves from one with complete time-reversal symmetry (Gaussian orthogonal ensemble) to one with no time-reversal symmetry (Gaussian unitary ensemble). The parameter γ may be related to the magnetic flux Φ through a two-dimensional dot having area A[17,18]

$$M\gamma^2=C\left(\frac{\Phi}{\Phi_0}\right)^2\frac{\hbar v_F}{\sqrt{A}\delta}, \tag{2.3}$$

where $\Phi_0=hc/e$ is the flux quantum, v_F is the Fermi velocity, and C is a constant of order unity.

The normal $(N_N+N_S)\times(N_N+N_S)$ scattering matrix $S(\varepsilon)$ of the system at an energy ε above E_F can be expressed in terms of the matrix H:[19]

$$S(\varepsilon)=1-2\pi i W^\dagger(\varepsilon-H-i\pi WW^\dagger)^{-1}W=\begin{pmatrix} r_{NN}(\varepsilon) & t_{NS}(\varepsilon)\\ t_{SN}(\varepsilon) & r_{SS}(\varepsilon)\end{pmatrix}, \tag{2.4}$$

where W is an $M\times(N_N+N_S)$ matrix representing the coupling between the point contacts and the dot, having elements

$$W_{mn}=\delta_{mn}\frac{1}{\pi}(2M\delta)^{1/2}\left(\frac{2-T_n-2\sqrt{1-T_n}}{T_n}\right)^{1/2}=\delta_{mn}\left(\frac{\lambda}{\pi}Z_n\right)^{1/2}. \tag{2.5}$$

The T_n are the transmission probabilities for each mode, which we take simply as T_N for modes coupled to the normal electrode and T_S for those coupled to the superconducting electrode (this in turn defines Z_N and Z_S).

For voltages below the excitation gap Δ of the superconductor, electrons and holes incident on the dot-superconductor interface may be Andreev reflected. In this case scattering from the dot, as seen from the normal metal contact, can be represented by a $2N_N\times 2N_N$ scattering matrix $\mathcal{S}$:

$$\mathcal{S}=\begin{pmatrix} r_{ee}(\varepsilon) & r_{eh}(\varepsilon)\\ r_{he}(\varepsilon) & r_{hh}(\varepsilon)\end{pmatrix}. \tag{2.6}$$

Here, $r_{he}(\varepsilon)$ is the $N_N\times N_N$ matrix describing the Andreev reflection of an incoming electron in the N point contact to an outgoing hole in the same lead; $r_{eh}(\varepsilon)$, $r_{ee}(\varepsilon)$, and $r_{hh}(\varepsilon)$ are defined analogously. These matrices may be written in terms of the submatrices of the normal scattering matrices $S(\varepsilon)$.[2] For $r_{he}(\varepsilon)$ one has

$$r_{he}(\varepsilon)=t_{NS}^*(-\varepsilon)M_{ee}(\varepsilon)\alpha(\varepsilon)t_{SN}(\varepsilon), \tag{2.7}$$

with

$$M_{ee}(\varepsilon)=[1-\alpha(\varepsilon)^2r_{SS}(\varepsilon)r_{SS}^*(-\varepsilon)]^{-1},$$

$$\alpha(\varepsilon)=\exp[-i\arccos(\varepsilon/\Delta)].$$

For voltages below the gap Δ in the S electrode, the zero temperature conductance of the system is given by the Tabikane-Ebisawa formula[20]

$$G(eV)=\frac{4e^2}{h}\mathrm{tr}\,r_{he}^\dagger(eV)r_{he}(eV). \tag{2.8}$$

We wish to calculate the ensemble-averaged Andreev conductance of the dot for arbitrary values of voltage V and magnetic field B; previous studies focused exclusively on the cases where V,B were 0 or large enough to completely break the symmetry between electrons and holes. To this end, we first rewrite Eq. (2.6) in a manner that is formally equivalent to the normal state expression (2.4). Letting $\Omega_S=\pi W_SW_S^\dagger$ and $\Omega_N=\pi W_NW_N^\dagger$, we define the $2M\times 2M$ effective particle-hole Hamiltonian[4,8]

$$\mathcal{H}=\begin{pmatrix} H & 0\\ 0 & -H^*\end{pmatrix}, \tag{2.9}$$

and the self-energies from the leads

$$\Sigma_N^0(\varepsilon)=-i\begin{pmatrix}\Omega_N & 0\\ 0 & \Omega_N\end{pmatrix},$$

$$\Sigma_S^0(\varepsilon)=-\frac{\Delta}{\sqrt{\Delta^2-\varepsilon^2}}\begin{pmatrix}(\varepsilon/\Delta)\Omega_S & \Omega_S\\ \Omega_S & (\varepsilon/\Delta)\Omega_S\end{pmatrix}. \tag{2.10}$$

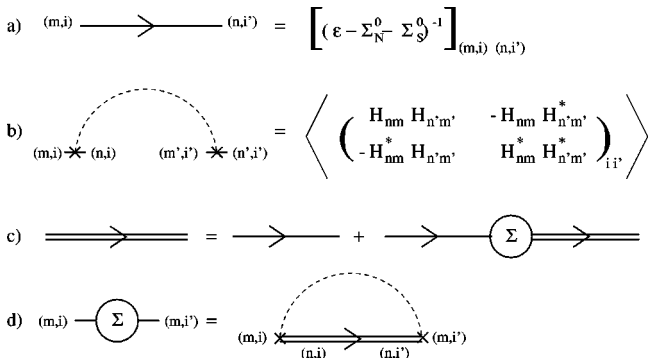

FIG. 2. (a) Definition and diagrammatic representation of the unaveraged Green function. This is a $2M\times 2M$ matrix; n,m refer to mode indices, while i,i' are electron-hole indices which can take one of two values (e or h). (b) The effective Hamiltonian $\mathcal{H}$ is represented by a cross; the dashed lines indicates averaging. (c) Diagrammatic Dyson equation; the double line is the averaged Green function $\langle\mathcal{G}\rangle$. (d) Self-energy to leading order in $1/M$; the neglected higher order terms correspond to graphs with crossed dashed lines. The intermediate index m is to be summed over. Note that Σ and hence $\langle\mathcal{G}\rangle$ are diagonal in mode space but have off-diagonal terms in particle-hole space.

With these definitions in place, a direct algebraic manipulation shows that the particle-hole scattering matrix $\mathcal{S}$ in Eq. (2.6) can be expressed in terms of the effective retarded Green function $\mathcal{G}_R$,

$$\mathcal{G}_R(\varepsilon)=[\varepsilon-\mathcal{H}(\varepsilon)-\Sigma_N^0(\varepsilon)-\Sigma_S^0(\varepsilon)]^{-1}, \qquad (2.11)$$

by

$$\mathcal{S}(\varepsilon)=1-2\pi i\begin{pmatrix} W_N^\dagger & 0\\ 0 & W_N^\dagger\end{pmatrix}\mathcal{G}_R(\varepsilon)\begin{pmatrix} W_N & 0\\ 0 & W_N\end{pmatrix}. \qquad (2.12)$$

The major simplification offered by Eq. (2.12) compared to Eq. (2.6) is that it allows one to compute the conductance in a manner analogous to that used in the normal state, as we now demonstrate. From this point onward, we focus on the case $\Delta\gg\varepsilon,eV$. In this regime, the properties of the system become independent of the specific details of the superconductor. Calculations retaining a finite Δ will be presented elsewhere.[21]

B. Details of the calculation: $B=0$

We proceed to average Eq. (2.8) for the Andreev conductance over the Gaussian orthogonal ensemble defined by Eq. (2.1), which is the appropriate ensemble for zero magnetic field. We make use of the relation

$$\langle H_{ij}H_{kl}\rangle=(\delta_{ik}\delta_{jl}+\delta_{il}\delta_{jk})\frac{\lambda^2}{M}. \qquad (2.13)$$

By expressing the scattering matrix in terms of the Green function $\mathcal{G}$, the trace appearing in the conductance formula may be represented as a standard ''conductance bubble'' diagram (see Fig. 3 below). Further, at this stage of the calculation λ^2/M is taken to be a small parameter, meaning that the usual diagrammatic technique for impurity averaging may be used. To obtain the leading-order result in $1/N_N,1/N_S$, we need only sum diagrams that have no crossed lines [lines indicate the averaging of matrix elements of H using the rule (2.13); see Fig. 2 above]. Note that λ will be sent to infinity only at the very end of the calculation; this procedure corresponds to first taking the matrix size to infinity while keeping a finite bandwidth, and then *independently* taking the bandwidth to infinity. This ordering of limits is necessary to generate a well-defined perturbative expansion.

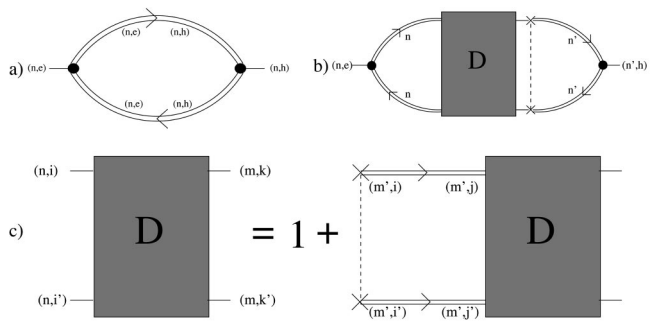

FIG. 3. (a) Direct contribution to the Andreev conductance. The trace appearing in Eq. (2.8) is represented by the bubble diagram. The double lines indicate the averaged Green function $\langle\mathcal{G}\rangle$. The index n corresponds to a mode coupled to the normal contact and should be summed over. (b) Diffusion contribution to the Andreev conductance. (c) Dyson equation for the $4M\times 4M$ matrix D. Note that upper and lower branches need to have matching mode indices, but not matching particle-hole indices.

The first step in this framework is to calculate the averaged matrix Green function $\langle\mathcal{G}\rangle$. As in Refs. 5 and 8, we find the following self-consistent Dyson equation:

$$\langle\mathcal{G}(\varepsilon)\rangle=[\varepsilon-\Sigma_N^0(\varepsilon)-\Sigma_S^0(\varepsilon)-\Sigma(\varepsilon)]^{-1}, \qquad (2.14a)$$

where the self-energy from averaging Σ is given by

$$\Sigma=1_M\otimes\begin{pmatrix}\Sigma_{ee} & \Sigma_{eh}\\ \Sigma_{he} & \Sigma_{hh}\end{pmatrix}=1_M\otimes\frac{\lambda^2}{M}\begin{pmatrix}\langle\mathrm{tr}\,\mathcal{G}_{ee}\rangle & -\langle\mathrm{tr}\,\mathcal{G}_{eh}\rangle\\ -\langle\mathrm{tr}\,\mathcal{G}_{he}\rangle & \langle\mathrm{tr}\,\mathcal{G}_{hh}\rangle\end{pmatrix}. \qquad (2.14b)$$

In this equation, 1_M denotes the $M\times M$ unit matrix, and $\otimes$ denotes a direct product; it is pictured diagrammatically in Fig. 2. Having performed the summation of diagrams, we now let $M\rightarrow\infty$, keeping ε,δ,N_S, and N_N fixed.

Three of the equations thus obtained relate the components of the self-energy to one another:

$$\Sigma_{ee}=\Sigma_{hh}, \quad \Sigma_{eh}=\Sigma_{he}, \qquad (2.15a)$$

$$\Sigma_{eh}^2-\Sigma_{ee}^2=\lambda^2. \qquad (2.15b)$$

The last equation allows us to parametrize Σ in terms of a pairing angle $\theta(\varepsilon)$:

$$\lambda\sin\theta(\varepsilon)=-\Sigma_{eh}(\varepsilon), \qquad (2.16a)$$

$$\lambda\cos\theta(\varepsilon)=i\Sigma_{ee}(\varepsilon). \qquad (2.16b)$$

The remaining self-energy equations now take the form

$$\tan[\theta(\varepsilon)]=\frac{N_SQ_S}{N_NQ_N-i\pi\varepsilon/2\delta}, \qquad (2.17a)$$

$$Q_N=\frac{T_N}{2}\{2-T_N[1-\cos\theta(\varepsilon)]\}^{-1}, \tag{2.17b}$$

$$Q_S=\frac{T_S}{2}\{2-T_S[1+\sin\theta(\varepsilon)]\}^{-1}. \tag{2.17c}$$

To obtain a unique solution of the self-energy equations we have imposed the boundary condition $\Sigma_{ee}(\varepsilon)\rightharpoonup -i\lambda$ as $\varepsilon\rightharpoonup\infty$; this represents the physical condition that we recover a normal metal with a constant density of states at large energies. The pairing angle θ can is related the density of states of the dot:

$$\rho(\varepsilon)=-\frac{\mathrm{Im}}{\pi}\mathrm{tr}\,\langle\mathcal{G}(\varepsilon+0^+)\rangle=\frac{\mathrm{Re}\{\cos[\theta(\varepsilon)]\}}{\delta}; \tag{2.18}$$

$\theta=\pi/2$ corresponds to a fully superconducting state, while $\theta=0$ corresponds to the normal state. It is interesting to note the analogy between $\theta(\varepsilon)$ and the pairing angle used in the quasiclassical theory of dirty normal-superconducting interfaces[22] and in the circuit theory of Andreev conductance.[23] In the present case, the normalization condition (2.15b) does not need to be externally imposed, but is a direct consequence of the averaging procedure.

While the leading-order solution of the self-energy Σ is sufficient if one is interested only in the density of states (as in Ref. 8), the conductance calculation requires that N_S/M, N_N/M, and $\varepsilon/M\delta$ corrections to Eq. (2.15b) be calculated. This correction may be expressed in terms of the leading-order self-energy solution:

$$\frac{\Sigma_{eh}^2-\Sigma_{ee}^2}{\lambda^2}-1=-\frac{1}{M}\Big(N_SQ_S[\sin(\theta)+Z_S]+N_NQ_N[\cos(\theta)+Z_N]+i\frac{\pi\varepsilon}{2\delta}\Big). \tag{2.19}$$

Having computed the self-energy from averaging Σ and thus the average Green function $\langle\mathcal{G}\rangle$, we can proceed to sum diagrams for the conductance. In analogy to the usual impurity technique,[24] two sets of contributions arise [see Fig. 3(a)] to leading order: $G=(4e^2/h)(g_{\mathrm{Dir}}+g_{\mathrm{Diff}})$. The first is a direct contribution which is completely determined by $\langle\mathcal{G}\rangle$, that is, by the ensemble-averaged probability amplitude $\langle r_{he}\rangle$:

$$g_{\mathrm{dir}}=(2\pi)^2\,\mathrm{tr}\;W_N^\dagger\langle\mathcal{G}\rangle W_NW_N^\dagger\langle\mathcal{G}\rangle^\dagger W_N=\mathrm{tr}\,\langle r_{he}\rangle\langle r_{he}\rangle^\dagger. \tag{2.20}$$

This contribution may be interpreted as arising from Andreev reflections that effectively occur at the interface of the normal lead and the cavity. The second contribution is due to the fluctuations of r_{he}:

$$g_{\mathrm{diff}}=\langle(r_{eh}-\langle r_{eh}\rangle)(r_{eh}-\langle r_{eh}\rangle)^2\rangle. \tag{2.21}$$

It describes the current carried by quasiparticles in the dot that are Andreev reflected at the interface of the dot and the superconductor. Diagrammatically, it is equivalent to a diffusion ladder, where the averaging links the upper and lower branches of the conductance bubble [see Figs. 3(b)–3(d)].[25] We ignore here quantum corrections, which are formally smaller by a factor of $\max(1/N_N,1/N_S)$. Note that in computing the diffusion sum each individual graph is of order $1/M$; this means that terms of order $1/M$ must be retained when computing the 4×4 matrix inverse arising from summing the series. As with the calculation of the average Green function $\langle\mathcal{G}\rangle$, we let M tend to infinity only after having performed the partial summation of diagrams.

To present the results of the conductance calculation, we first define the following kernel functions:

$$\Lambda(\varepsilon)=2N_N\Big(1-\Big|\frac{Q_N}{Z_N}\Big|^2|1+Z_N\cos(\theta)|^2\Big)+2N_S\Big(1-\Big|\frac{Q_S}{Z_S}\Big|^2|1+Z_S\sin(\theta)|^2\Big)-2\,\mathrm{Re}\{N_NQ_N[Z_N+\cos(\theta)]+N_SQ_S[Z_S+\sin(\theta)]\}+\frac{\pi\varepsilon}{\delta}\mathrm{Im}\,[\cos(\theta)], \tag{2.22a}$$

$$\Omega(\varepsilon)=2N_N|Q_N\sin(\theta)|^2+2N_S|Q_S\cos(\theta)|^2, \tag{2.22b}$$

$$\Pi_N(\varepsilon)=2N_N|Q_N|^2\{(1+6Z_N^2+Z_N^4)[1+|\cos(\theta)|^2]+8Z_N(1+Z_N^2)\mathrm{Re}[\cos(\theta)]\}, \tag{2.22c}$$

$$\Pi_S(\varepsilon)=2N_S|Q_S|^2\{(1+6Z_S^2+Z_S^4)[1+|\cos(\theta)|^2]+8Z_S(1+Z_S^2)\mathrm{Re}[\cos(\theta)]\}, \tag{2.22d}$$

where Z_N and Z_S were defined below Eq. (2.5). With these definitions, we find

$$g_{\mathrm{dir}}=2N_N\frac{T_N^2}{|2-2T_N\sin^2(\theta/2)|^2}|\sin(\theta)|^2, \tag{2.23a}$$

$$g_{\mathrm{diff}}=8N_N^2\Big|\frac{Q_N^2}{Z_N}\Big|^2(\Lambda^2-\Omega^2)^{-2}[\Pi_N|\sin(\theta)|^2+(1-Z_N^2)^2\Lambda|\sin(\theta)|^2+\Pi_S|\cos(\theta)|^2]. \tag{2.23b}$$

Equations (2.22a)–(2.23b), along with Eq. (2.17) for the self-energy Σ, determine the ensemble-averaged $B=0$ Andreev conductance through the dot to leading order in $1/N_N,1/N_S$ for all voltages such that $eV\ll\Delta$. The extension of these formulas to nonzero B is presented in the Appendix.

III. PROBING INDUCED SUPERCONDUCTIVITY VIA CONDUCTANCE

A. Chaotic dot

In this section, we consider the situation where the coupling between the dot and the superconductor is much stronger than the coupling between the dot and the normal lead, $N_NT_N\ll N_ST_S$. In this limit, the normal metal will only weakly perturb the properties of the dot-superconductor system; thus, we may view the conductance through the struc-

ture as being a probe of the induced superconductivity in the dot. As mentioned in the Introduction, previous studies have examined the density of states of such Andreev billiards in the absence of a normal lead.[5] It was found for the case of a chaotic dot that an energy gap $\tilde{\Delta}$ opens up on a scale set by the inverse of the time needed for a particle to escape from the dot to the superconductor:

$$\tilde{\Delta} = c(E_S), \tag{3.1}$$

$$E_S = \left(\frac{\hbar}{\tau_{S\ \mathrm{esc}}} \right) = \left(\frac{N_S T_S \delta}{2\pi} \right). \tag{3.2}$$

The parameter c is of order unity and a monotonic function of T_S; it varies from 0.6 in the case of no tunnel barrier to 1 in the case of an opaque tunnel barrier. It was also found that the shape of the density of states above $\tilde{\Delta}$ was vastly different in these two limits: in the tunnel regime $T_S \ll 1$, the density of states was BCS-like, having a square-root singularity at $\tilde{\Delta}$, whereas in the case of no tunnel barrier the density of states gradually increased above $\tilde{\Delta}$. Note that the gap $\tilde{\Delta}$ does not depend on the gap Δ in the bulk superconductor, which was taken to infinity in the calculations.

The question that naturally arises here is how the induced superconductivity seen in the density of states manifests itself in the conductance. Some insight may be obtained by considering Eqs. (2.23a) and (2.23b) to lowest order in the small parameter $\eta = N_N T_N / N_S T_S$. Without the normal lead, we have a gap in the dot density of states up to an energy $\tilde{\Delta}$. As the density of states is proportional to $\mathrm{Re}\{\cos[\theta(\varepsilon)]\}$, this implies that $\mathrm{Re}[\theta(\varepsilon)] = \pi/2 + O(\eta)$ for $\varepsilon < \tilde{\Delta}$. Using this, the ''subgap'' (i.e., $\varepsilon < \tilde{\Delta}$) direct contribution to the conductance takes the form

$$g = g_{\mathrm{dir}}(\varepsilon) = \frac{2N_N T_N^2}{(2-T_N)^2 - 4(1-T_N)(\mathrm{Im}\{\sin[\theta_0(\varepsilon)]\})^2} + O(\eta), \tag{3.3}$$

while the diffusion contribution g_{Diff} is of order η^2 and thus negligible. As the energy is increased above the gap, the density of states returns to its normal state value, and consequently $\theta(\varepsilon) \to 0$ to leading order. For $\varepsilon \gg \tilde{\Delta}$ the direct term is negligible [being proportional to $\sin(\theta)$], while the diffusion term gives the normal state conductance:

$$g = g_{\mathrm{diff}}(\varepsilon) = N_N T_N + O(\eta). \tag{3.4}$$

The above considerations become extremely suggestive when one considers the case $T_N = 1$. There is a perfect conductance doubling for voltages below the effective gap $\tilde{\Delta}$, while at higher voltages the conductance drops to its normal state value:

$$g = \begin{cases} 2N_N & \text{for } \varepsilon \ll \tilde{\Delta} \\ N_N & \text{for } \varepsilon \gg \tilde{\Delta}. \end{cases} \tag{3.5}$$

This is precisely what would be expected *if* the normal point contact were in perfect contact with a bulk superconductor having a gap $\tilde{\Delta}$—conductance doubling would be expected below the gap due to Andreev reflection, whereas above the gap the normal state conductance would be recovered as quasiparticles would now carry the current. In this respect, note that below the induced gap $\tilde{\Delta}$ both the averaged reflection probability $\langle |r_{eh}|^2 \rangle$ *and* the averaged reflection amplitude $|\langle r_{eh} \rangle|$ are nonzero; for $eV \gg \tilde{\Delta}$, the latter vanishes. Nonetheless, in both cases (i.e., for voltages above and below $\tilde{\Delta}$), Andreev reflection is the only current carrying process. For energies below $\tilde{\Delta}$, the dot itself appears as if it were superconducting and Andreev reflection effectively occurs at the normal-lead–dot interface. For energies far above $\tilde{\Delta}$, current through the dot is effectively carried by quasiparticles in the dot (which are either electron- or holelike) which Andreev reflect at the dot-superconductor interface.

The quantum dot continues to act as if it were a superconductor in the case where the contact to the normal lead is no longer perfect (i.e., $T_N \neq 1$); one need only note that, if $\mathrm{Im}\{\sin[\theta_0(\varepsilon)]\}$ is replaced by $\varepsilon/\tilde{\Delta}$, Eq. (3.3) becomes identical to the Blonder-Tinkham-Klapwijk (BTK) formula for the subgap conductance of a normal-point-contact–superconductor junction, where there is a tunnel barrier at the interface having transmission T_N.[26] The BTK formula is derived assuming there is no spatial separation between the sites of Andreev scattering and normal scattering; the only energy dependence thus comes from the Andreev reflection phase $\alpha(\varepsilon)$, not from the lack of electron hole degeneracy at finite voltages. The replacement of $\varepsilon/\tilde{\Delta}$ by $\mathrm{Im}\{\sin[\theta_0(\varepsilon)]\}$ in Eq. (3.3) means that the Andreev reflection phase $\tilde{\alpha}$ in the present case is not necessarily the usual $\alpha(\varepsilon)$ given in Eq. (2.7), but is rather defined through

$$\mathrm{Im}\{\sin[\theta_0(\varepsilon)]\}^2 = \frac{1 + \mathrm{Re}[\tilde{\alpha}(\varepsilon)^2]}{2}. \tag{3.6}$$

This notwithstanding, the overall implication is still that for $eV \ll \tilde{\Delta}$ we can effectively consider all Andreev reflections as occurring at the N-dot interface rather than at the dot-S interface—the dot is indeed acting as though it were itself a superconductor.

We have numerically solved Eqs. (2.17a)–(2.17c) for the pairing angle $\theta(\varepsilon)$, and used this to compute the Andreev conductance versus voltage. In Figs. 4 and 5, we plot the calculated conductance vs voltage curves for various values of T_N, and compare to what would be expected from the BTK theory for a simple N-S interface. We find an excellent agreement in the case of $T_S \ll 1$ (see Fig. 4) even for voltages above the gap $\tilde{\Delta}$ in the dot. Such an agreement is not unlikely, as for $T_S \ll 1$ the dot density of states is BCS-like, and consequently the effective Andreev phase $\tilde{\alpha}$ is just equal to the usual Andreev phase α. In the opposite case of a transparent contact to the superconductor (Fig. 5), clear deviations from the BTK line shapes are seen. These deviations result completely from the fact that $\tilde{\alpha} \neq \alpha$, which is to be expected as the dot density of states in this case is quite different from the BCS form.

The ''induced superconductivity'' effect in the dot also manifests itself in other ways. A straightforward calculation in the limit $T_N \to 0$ shows that the Andreev conductance becomes proportional to the dot density of states, i.e.,

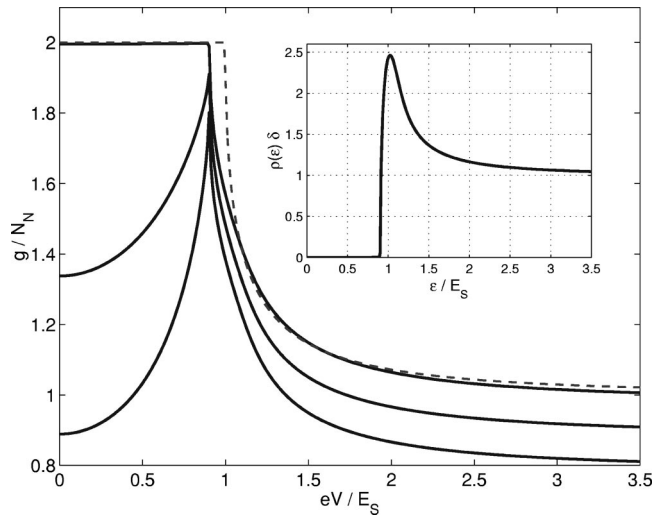

FIG. 4. Conductance versus voltage for $N_S=10^4N_N$, $T_N=0.1$, illustrating the ''local Andreev reflection'' effect, in which the dot itself acts as a superconductor having a gap $\tilde{\Delta}$. Solid lines are calculated curves for, from top to bottom, $T_N=1,0.9,0.75$. The dashed curve shows the BTK result for $T_N=1.0$; close agreement is found for all values of T_N. The dot density of states (shown in the inset) in this case resembles a BCS density of states. The voltage is measured in units of E_S, the inverse of the escape time to the superconductor [cf. Eq. (3.2)].

Re$[\cos(\theta)]$; thus, the Andreev conductance becomes equivalent to a conventional superconductor tunneling density of states measurement. We have also calculated the magnetic field dependence of the Andreev conductance in the limit of small η (see the Appendix); here too, our results are consistent with a picture in which the dot itself acts as a superconductor. The conductance enhancement at zero field remains constant until a critical flux Φ_C given by

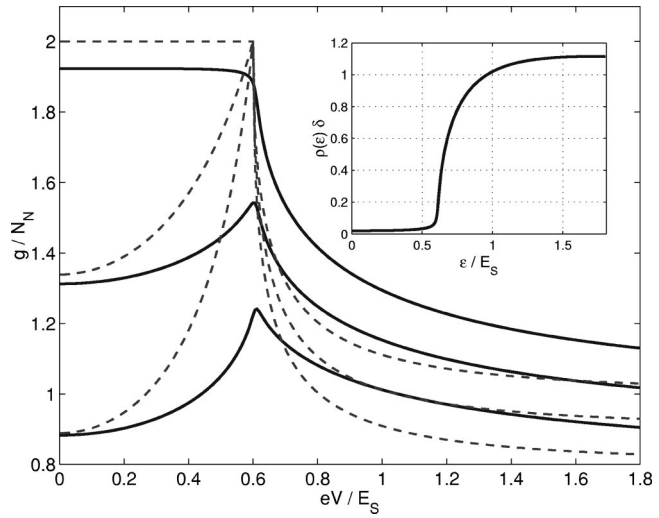

FIG. 5. Conductance versus voltage for $N_S=10^4N_N$, $T_S=1$, illustrating the ''local Andreev reflection'' effect. Solid lines are calculated curves for, from top to bottom, $T_N=1,0.9,0.75$; dashed curves show BTK result for same values of T_N. The differences in the dot density of states (shown in the inset) from a BCS density of states lead to large differences from the BTK line shapes.

$$\left(\frac{\Phi_C}{\Phi_0}\right)=C\sqrt{\frac{\tilde{\Delta}}{E_{\rm erg}}}=C\sqrt{\frac{\tilde{\Delta}\tau_{\rm erg}}{\hbar}}, \tag{3.7}$$

where $\tau_{\rm erg}$ is the ergodic time and C is a geometry dependent constant of order unity. This is the same critical field required to close the gap $\tilde{\Delta}$. Note that, unlike a conventional BCS superconductor, where the critical field is proportional to the gap, in the present case Eq. (3.7) implies that the critical field is proportional to $\sqrt{\tilde{\Delta}}$.

The conclusions reached here are markedly different from what would be expected from a naive trajectory-based semiclassical analysis.[27] Consider the situation of a ballistic dot with no tunnel barriers, where $N_S \gg N_N$. In the semiclassical picture, electrons entering the dot from the normal lead typically bounce off the walls of the dot several times before hitting the superconductor, where they Andreev reflect. At $V=0$, holes are the time-reversed partners of electrons; thus, when an Andreev reflection occurs, the hole will retrace the path of the incoming electron *and* cancel its acquired phase. Andreev trajectories will thus interfere constructively, leading to a large conductance enhancement at $V=0$ and a nonvanishing average reflection amplitude $\langle r_{he}\rangle$. This enhancement should be lost, however, as the voltage is increased—at finite V, electrons and holes are no longer degenerate, and the phase acquired by the hole will not precisely cancel that acquired by the electron. The presence of a residual phase $\delta\phi=eVL/(\hbar v_F)$ (where L is the length of the trajectory) will lead to destructive interference and a consequent decrease in the conductance. In this picture, even a small voltage should impair the conductance enhancement seen at zero voltage.

To make this picture quantitative, we may use the fact that our exact random matrix theory indicates that the conductance below $\tilde{\Delta}$ is proportional to $|\langle r_{he}\rangle|^2$ [see Eq. (3.3)]. Using the semiclassical Andreev phase $\delta\phi=eVL/(\hbar v_F)$ and the fact that path lengths in chaotic systems have an exponential distribution function $P(L)=\exp(-L/\bar{L})/\bar{L}$,[28] we estimate the average of the semiclassical reflection amplitude as

$$\langle r_{he}\rangle_{\rm SC}\simeq\int dL e^{ieVL/\hbar v_F}P(L)=\frac{1}{1-ieV\bar{L}/\hbar v_F}, \tag{3.8}$$

where $\bar{L}$ is the mean path length to the superconductor; for a ballistic dot, we have $\bar{L}=v_F\tau_{S\ \rm esc}$. Hence,

$$|\langle r_{he}\rangle|^2=\left[1+\left(\frac{eV}{c\tilde{\Delta}}\right)^2\right]^{-1}, \tag{3.9}$$

where we have used $\tilde{\Delta}=c\hbar/\tau_{S\ \rm esc}$ [see Eq. (3.1)] with $c\simeq 0.6$ in the case of a perfect contact to the superconductor. The semiclassical approach thus predicts that $|\langle r_{he}\rangle|^2$ (and hence the Andreev conductance) will fall off with voltage as a Lorentzian for $eV<\tilde{\Delta}$. This is clearly at odds with our fully quantum mechanical calculation at $T_N=1$, which shows that $|\langle r_{he}\rangle|^2=1$ for all voltages below $\tilde{\Delta}$. We return to the discrepancy between the semiclassical and quantum mechanical calculations in the next subsection.

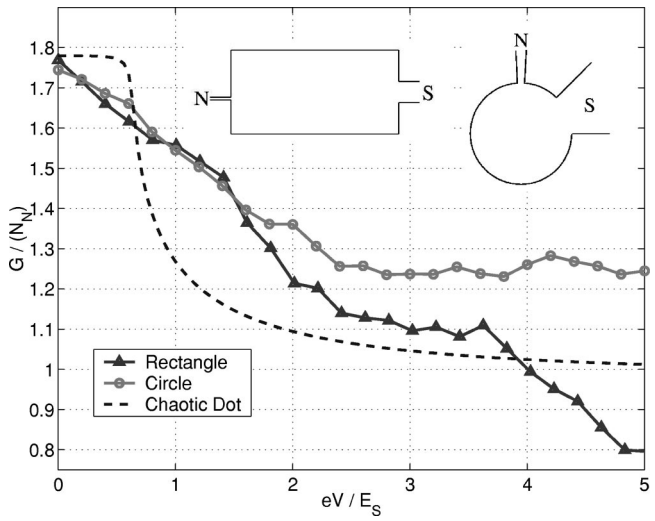

FIG. 6. Conductance (scaled by N_N) vs voltage for a rectangular dot and a circular dot, each with $N_N=10$, $N_S=30N_N$ (shapes shown in the inset, with the size of the normal lead exaggerated). Each plot was produced by averaging over small variations in E_F. Unlike a chaotic dot (dashed line), the Andreev conductance of the integrable dots has no ''plateau'' for $eV<\tilde{\Delta}$. The conductance of the rectangle drops below N_N due to a weak localization correction. The energy scale E_S is defined in Eq. (3.2).

B. Integrable Dot

In this subsection, we examine the conductance of a N-dot-S system where the classical dynamics of the dot are integrable. Previous studies[5,7] have indicated that the proximity effect in the density of states is very different for chaotic and integrable billiards; in the latter, there is no induced gap, but rather the density of states tends to zero linearly at E_F. We argue here that the proximity effect's strong sensitivity to chaos versus integrability also manifests itself in the Andreev conductance.

We consider two different integrable systems: a rectangular dot and a circular dot. In each case, the dot is coupled via narrow leads to both a normal metal and a superconductor; there are no tunnel barriers. As in the previous subsection, we consider the case where the width of the normal contact is much smaller than the width of the superconducting contact (see the inset of Fig. 6), so that the normal contact serves as a probe of the proximity effect in the quantum dot. The scattering matrix of the system is computed by numerically matching wave functions across the structure, and the conductance then follows from Eq. (2.8). The number of modes in the normal lead was fixed at $N_N=\mathrm{int}(k_F W/\pi)$;[29] we averaged results over small variations in k_F, which did not change N_N. Our results are displayed in Fig. 6; similar results are obtained if one changes the positions of the two point contacts.

The results for the two integrable systems are similar to one another, and differ significantly from what was found for a chaotic dot—as opposed to a flat subgap region followed by a rapid drop-off, we have instead a gradual linear reduction of the conductance with voltage. We argue that the difference exhibited here is generic for integrable systems. The reason is the same as that given in Ref. 5 to explain the difference in density of states, namely, that the distribution of path lengths is very different for integrable and chaotic dynamics.[28] In the first case, there is a power law distribution of path lengths, meaning that there is an appreciable probability of finding long paths. Even for small voltages, these long paths will quickly acquire a random phase, leading to destructive interference and a reduction of the conductance. In contrast, chaotic systems have an exponential distribution of path lengths—long paths are quite rare. In this case, small voltages will not be able to cause any significant phase randomization, and thus there will be no resulting destructive interference of Andreev trajectories.

Although the semiclassical reasoning in terms of path lengths presented here provides a qualitative account for the difference between the chaotic and integrable Andreev conductance line shapes, attempts to translate it into a quantitative theory have not been successful. As was demonstrated in the previous section, a simple semiclassical theory for the chaotic case fails to recover the correct line shape. A similar problem is encountered when one tries to do the analogous calculation for the integrable case—such a calculation predicts that the Andreev conductance should fall off quadratically with voltage, albeit at a faster rate than in the chaotic case. This behavior is clearly at odds with our exact calculation showing a linear dependence on voltage. In many ways, the failure of a semiclassical approach is not surprising. It is known that semiclassical approximations are unreliable in superconducting systems, as the usual diagonal approximation is worse than for normal systems.[5,7]

Finally, we note that there is a striking connection between the Andreev conductance's sensitivity to the nature of the dot's classical dynamics and weak localization. It has been shown both theoretically[30] and experimentally[31] that the magnetic field dependence of the weak localization correction of a quantum dot with two normal leads is very different for chaotic versus integrable dots. In the chaotic case, one finds a smooth Lorentzian field dependence, while in the integrable case a much sharper profile is found, with a cusp at zero magnetic field. The similarity between the Andreev conductance effect and that in weak localization is not coincidental; both effects rely on the interference of time-reversed paths.

Despite this strong similarity, it is worth noting that the effect in the Andreev conductance is much more pronounced. Here, the difference between the chaotic and integrable line shapes is more severe than in the weak localization effect (i.e., the chaotic case is much flatter than a Lorentzian). The magnitude of the effect is also much larger in the Andreev case; the signature of chaos versus integrability is the *entire conductance* itself, not a quantum correction like weak localization. For this reason, the effect in the Andreev conductance should be observable in a single sample, whereas an ensemble average is required in the weak localization case.

IV. REENTRANCE EFFECTS

We shift focus in this section, and examine so-called reentrance phenomena in the Andreev conductance of a chaotic quantum dot. These effects are loosely defined by nonmonotonic behavior of the conductance in either voltage or magnetic field. They are well known in the case of diffusive NS systems,[13,14] where the word ''reentrant'' is used because the

Andreev conductance is the same as the normal conductance at zero voltage and magnetic field, and at high voltage or field, but *not* for intermediate values. The theory developed here allows us to address this behavior using a scattering approach, whereas previous approaches almost exclusively made use of the quasiclassical Green function technique. In what follows, we discuss the cases of ballistic contacts ($T_N = T_S = 1$) and tunnel contacts ($T_N, T_S \ll 1$) separately.

A. Ballistic contacts

In the absence of tunnel junctions, the equations determining the conductance simplify considerably. We find

$$g_{\rm dir}(\varepsilon) = 2N_N \tan^2\left(\frac{\theta(\varepsilon)}{2}\right), \tag{4.1}$$

$$g_{\rm diff}(\varepsilon) = \frac{N_N^2}{2}\left|\cos\left(\frac{\theta(\varepsilon)}{2}\right)\right|^{-4} \frac{N_N|\tan[\theta(\varepsilon)/2]|^2 + N_S|\cos[\theta(\varepsilon)]/\{1+\sin[\theta(\varepsilon)]\}|^2}{\Lambda(\varepsilon)^2 - \Omega(\varepsilon)^2}. \tag{4.2}$$

As discussed in the previous section, these two contributions to the Andreev conductance can be interpreted as representing two distinct physical consequences of the proximity effect. The direct term $g_{\rm dir}$ represents processes in which the dot mimics a bulk superconductor, with Andreev reflections effectively occurring locally at the N-dot interface. It *decreases monotonically* with voltage and magnetic field, going to zero at large voltages or magnetic fields. This reflects the fact that the induced superconductivity effect is sensitive to the averaged *amplitude* for Andreev reflection, which is largest at $V = B = 0$. On the other hand, the diffusion term $g_{\rm diff}$ *increases* monotonically with V and B, tending to the classical result for two conductances in series:

$$g_{\rm diff} \rightarrow g_{\rm class} = \frac{(2N_S)(N_N)}{2N_S + N_N}. \tag{4.3}$$

It represents a contribution from Andreev quasiparticles in the dot, and is thus sensitive to the dot's density of states. In the present case of ballistic contacts, the density of states does not have any BCS-type peak and thus the diffusion term rises steadily with applied V or B.

Given that the direct and diffusion contributions react in opposite fashions to an increase in V or B, it is not surprising that a nonmonotonic V or B dependence of the total conductance can be found if the relative strengths of these two terms are varied. The latter can be achieved by tuning the ratio of N_N/N_S. If $N_N \ll N_S$, the direct term will be dominant at $V, B = 0$, and we expect a monotonic decrease of G as a magnetic field or finite bias are applied. In the opposite limit $N_N \gg N_S$, the diffusion term dominates at $V, B = 0$, and G is expected to increase with V or B. A nonmonotonic V or B dependence can thus be anticipated in the intermediate regime where N_N and N_S are comparable.

To quantify the competition between the direct and diffusion contributions, we examine these terms at $V = B = 0$. This is done by solving the self-energy equations (2.15a)–(2.17c) to determine $\theta(\varepsilon)$, and then substituting this into Eqs. (4.1) and (4.2). Letting $N_{\rm sum} = \sqrt{N_N^2 + 6N_N N_S + N_S^2}$, we obtain

$$g_{\rm dir} = (N_{\rm sum} - N_S - N_N)\frac{N_{\rm sum}}{N_N} - 2N_S, \tag{4.4a}$$

$$g_{\rm diff} = (N_{\rm sum} - N_S - 3N_N)\frac{N_S}{N_N} + \frac{4N_N N_S}{N_{\rm sum}}, \tag{4.4b}$$

with the total conductance given by[12]

$$g = g_{\rm dir} + g_{\rm diff} = (N_S + N_N)\left(1 - \frac{N_N + N_S}{N_{\rm sum}}\right). \tag{4.5}$$

Plotted in Fig. 7 as a function of N_N/N_S are the zero field values of $g_{\rm dir}$, $g_{\rm diff}$, and g, normalized by the high field conductance given by the classical formula (4.3). As N_N/N_S is increased from zero, the total conductance initially decreases with $g_{\rm dir}$ as the local Andreev reflection effect is suppressed, while at larger values it starts to increase with $g_{\rm diff}$ as the density of states at E_F returns to its normal state value. At $N_N \simeq \frac{1}{2}N_S$, we find that the total conductance at zero field is the same as the classical result. Not surprisingly, we find that reentrance effects in both magnetic field and voltage are maximized here (see Fig. 8).

It is instructive to make a comparison at this point to the nonmonotonic reentrance behavior of diffusive NS systems (i.e., a diffusive normal metal in good contact with a superconductor). In the diffusive case, the zero field and high field conductances are the same, being equal to the normal state

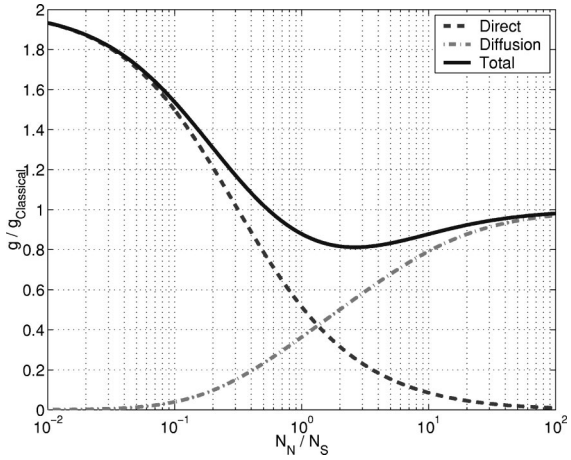

FIG. 7. Plot of the direct and diffusion contributions to the $V = 0, B = 0$ conductance as a function of N_N/N_S for transparent point contacts ($T_N = T_S = 1$). At $N_N \simeq N_N/2$, the total $V = 0, B = 0$ conductance is the same as the classical result $g_{\rm class}$.

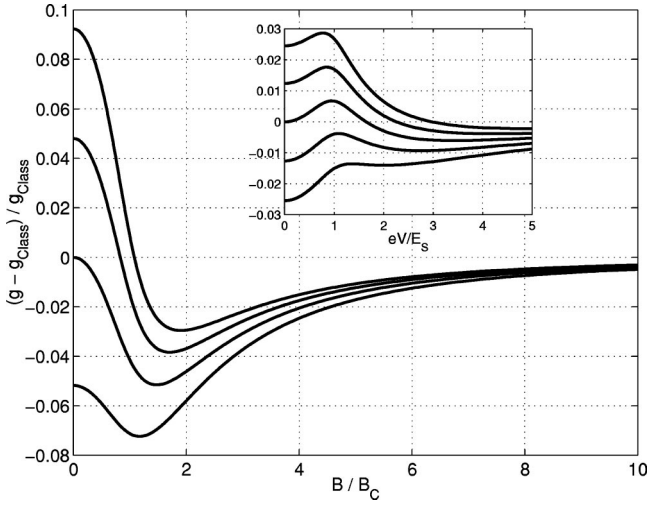

FIG. 8. Plot of the excess conductance $[g(B,V)-g_{\rm class}]/g_{\rm class}$ as a function of B at $V=0$, showing nonmonotonic behavior. From top to bottom, curves are for $N_N/N_S=0.39,0.45,0.54,0.68$. The inset shows the excess conductance at $B=0$ as a function of voltage; from top to bottom, curves are for $N_N/N_S=0.49,0.51,0.57,0.6$. In general, reentrance effects are maximized at $N_N/N_S\simeq 0.54$, where the $V=0,B=0$ conductance is the same as at large V or B.

conductance. The lack of any change due to superconductivity at $V=B=0$ is usually explained as an exact cancellation of the conductance doubling effect of Andreev reflection by a suppression of the density of states at the Fermi energy. A conductance enhancement is, however, found at finite voltage, roughly at $eV\simeq E_T=\hbar D/L^2$, where D is the diffusion constant and L is the length of the normal metal. Quasiclassical calculations find maximum conductance enhancements on the order of 10% of the normal state conductance.[13]

In the present system, we can tune the relative significance of the Andreev reflection enhancement and density of states suppression terms by varying N_N/N_S. We find that nonmonotonic effects are maximized when we adjust this ratio to mimic the diffusive system, by insisting that the zero field and high field conductances are the same; this occurs at $N_N\simeq 1/2N_S$. The conductance maximum in voltage is smaller however, being on the order of $0.01g_{\rm class}$, and occurs roughly at $eV=E_S=N_S\delta/2\pi$. This is the inverse of the time needed to escape to the superconductor, and is thus the analog of E_T in the diffusive system, which represents the inverse of the time needed for a particle to diffuse across the normal metal and reach the superconductor. Note also that if the normal lead is removed the size of the induced gap $\tilde{\Delta}$ in the dot density of states is $\sim E_S$.

Finally, we also find pronounced nonmonotonic behavior in magnetic field for this range of N_N/N_S, with the magnitude of the effect being larger than that in voltage (Fig. 8). The maximum conductance occurs roughly at a flux Φ_C given by Eq. (3.7), the same flux that would be required to close the gap in the density of states in the absence of the normal lead.

B. Tunnel regime

We turn now to the case where both point contacts contain opaque tunnel barriers ($T_S,T_N\ll 1$). In this regime, it is sufficient to consider the conductance to lowest nonvanishing order in T_N and T_S. Of particular interest here is the well-known ''reflectionless tunneling'' effect[27]—the $V=0,B=0$ Andreev conductance of a N-I-N-I-S structure (where I is an insulating region having transmission T) is found to be proportional to T, not to T^2 as one has for a single barrier. It is as though the Andreev reflected hole is not reflected at all by the tunnel barriers. A similar effect occurs for a N-I-S system where the normal region is sufficiently disordered. The origin of this striking behavior is now understood to be the constructive interference of trajectories that reflect many times between the two barriers, leading to a fraction $\sim T$ of the conductance channels being open (i.e., having a transmission probability close to unity).[32]

In the present case, we are able to examine the effects of finite voltage and magnetic field on reflectionless tunneling when a quantum dot separates the barriers. At large voltages or magnetic fields, the pairing angle $\theta(\varepsilon)$ tends to its normal state value of 0, and we find that the conductance is given to leading order by the classical series addition formula

$$g_{\rm class}=\frac{\left\langle \frac{1}{2}N_S T_S^2\right\rangle (N_N T_N)}{\frac{1}{2}N_S T_S^2+N_N T_N}. \tag{4.6}$$

For $N_S T_S^2\ll N_N T_N$, this simplifies to $g_{\rm class}=\frac{1}{2}N_S T_S^2$. Unlike the case at $V=0,B=0$, there is no order T reflectionless tunneling contribution here, as the necessary constructive interference is lost when electron-hole degeneracy or time-reversal symmetry is broken. Below we show that reflectionless tunneling does survive at small values of B and V, and describe how this contribution evolves as B and V are increased.

We begin by solving Eqs. (2.17a)–(2.17c) for the self-energy to lowest order in T_N,T_S for $B=0$; we find the pairing angle is given simply by

$$\theta(\varepsilon)=\arctan\left(\frac{E_S}{E_N-i\varepsilon}\right). \tag{4.7}$$

E_S and E_N are the inverse escape times to the superconductor and normal metal leads, respectively, and are defined by

$$E_N=\frac{N_N T_N\delta}{2\pi},\quad E_S=\frac{N_S T_S\delta}{2\pi}. \tag{4.8}$$

Using this result for $\theta(\varepsilon)$, we next write Eqs. (2.23a) and (2.23b) for the conductance to lowest order in T_S,T_N. The direct contribution $g_{\rm dir}$ corresponds to Andreev reflection at the N-dot interface and is of order T_N^2. The only order T contribution is found in the diffusion term $g_{\rm diff}$, which yields

$$g_{\rm diff}(\varepsilon)=N_N T_N\frac{E_N E_S^2}{\tilde{E}^2(\varepsilon)}\sqrt{\frac{2}{\tilde{E}^2(\varepsilon)+E_N^2+E_S^2-\varepsilon^2}}+O(T^2), \tag{4.9}$$

where we have defined

$$\tilde{E}(\varepsilon)=[(E_S^2-E_N^2-\varepsilon^2)^2+4(E_S E_N)^2]^{1/4}. \tag{4.10}$$

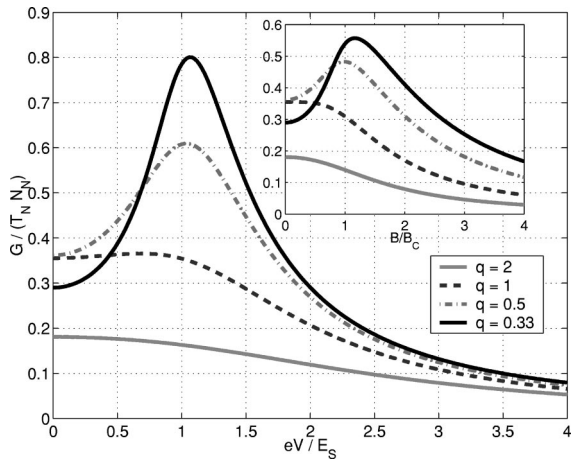

FIG. 9. Conductance vs voltage in the tunnel regime $T_N = T_S = 0.01$, exhibiting the enhancement of reflectionless tunneling at finite voltage. The parameter q is defined as the ratio N_N/N_S. The inset shows the $V=0$ conductance as a function of magnetic field for the same parameter choices.

Equation (4.9) gives the complete voltage dependence of the reflectionless tunneling effect. At $V=0$, it reduces to

$$g_{\mathrm{diff}}(0) = \frac{(N_N T_N)^2 (N_S T_S)^2}{[(N_N T_N)^2 + (N_S T_S)^2]^{3/2}}, \tag{4.11}$$

which is similar to the formula found in Ref. 32, generalized to the case where the point contacts have different widths. Depending on the relative magnitudes of E_S and E_N, the conductance drops monotonically with voltage, or shows a maximum around $eV \simeq E_S$ (see Fig. 9). The location of the maximum is at $eV = \sqrt{7/6} E_S$ if $E_S \gg E_N$. Similar behavior is found for the magnetic field dependence of the conductance (see the inset of Fig. 9).

It is easy to understand the origin of this nonmonotonic behavior within our theory. When N_S becomes larger than N_N, the effect of the superconductor on the dot density of states becomes significant. As we have seen in Sec. II, the induced density of states will have a sharp peak at E_S when $T_S \ll 1$; it is this peak that is manifesting itself in the conductance.

It is interesting to note that Eq. (4.9) has the same form as was found for a diffusive N-I-N-I-S system using a quasiclassical Green's function approach.[33] In that system, the quantum dot is replaced by a diffusive normal wire of length d, width W, and mean free path l, and the normal and superconducting leads are not attached via point contacts, but are also wires of the same width. In the limit $T_N, T_S \ll l/d$ the resistances of the tunnel barriers dominate, and an expression identical to Eq. (4.9) is obtained, but now the energies E_N, E_S are given by

$$E_N = T_N \frac{\hbar v_F}{4d}, \quad E_S = T_S \frac{\hbar v_F}{4d}, \tag{4.12}$$

where v_F is the Fermi velocity in the normal interbarrier region. This is identical to the definition of E_N and E_S in Eq. (4.8) if one takes δ to be the level spacing in the wire. Note that this correspondence is not surprising; previous studies have also found that adding strong tunnel barriers makes a diffusive normal wire with many channels equivalent to a quantum dot.

V. CONCLUSIONS

We have studied the voltage (V) dependence of the Andreev conductance of chaotic and integrable quantum dots; we have also examined the magnetic field (B) dependence in the chaotic case. In the regime where the contact to the superconductor dominates, we find that the voltage dependence of the Andreev conductance is extremely sensitive to the nature of the dot's classical dynamics—in the chaotic case, the dot itself mimics a superconductor and the conductance is initially flat in voltage, whereas in the integrable case the conductance falls off linearly with voltage. This effect is large in that the entire conductance forms the signature of chaos vs integrability; also, it does not require any ensemble averaging to be done. Both these facts make it particularly amenable to experiments using semiconductor quantum dots, where a good contact between dot and superconductor can be achieved in samples having a fixed dot shape.[34,35] These experiments typically employ Nb for the superconducting contact, while the quantum dot is defined in a two-dimensional electron gas residing in an InAs layer.

We have also studied nonmonotonic reentrance phenomena in the V and B dependence of the Andreev conductance of a chaotic dot. We find that such behavior is ubiquitous, and is the result of two competing processes—Andreev reflection at the dot–normal-lead interface, which decreases as V or B increases, versus quasiparticles being injected into the dot, which increases with V and B.

ACKNOWLEDGMENTS

We thank C. W. J. Beenakker for a useful discussion. A.C. acknowledges the support of the Olin Foundation and the Cornell Center for Materials Research. This work was supported in part by the NSF under Grant No. DMR-9805613.

APPENDIX: CALCULATING THE ANDREEV CONDUCTANCE FOR $B \neq 0$

In this Appendix, we outline the method used for calculations at nonzero magnetic field B. Formally, the magnetic field enters the model in a different fashion from a voltage difference. The latter is dealt with by the fact that the Andreev scattering matrix $\mathcal{S}$ defined in Eq. (2.12) is an explicit function of energy. The field dependence, however, does not appear directly in the expression for $\mathcal{S}$, but rather only emerges in the averaging procedure—as we use the Pandey-Mehta distribution defined in Eq. (2.2), the ensemble of random matrices is itself a function of field.

As in the calculation at $B=0$, the first step in obtaining the conductance is to calculate the averaged matrix Green function $\langle \mathcal{G} \rangle$ defined in Eq. (2.14a). The diagrams used are the same as in the $B=0$ case, but now use of the distribution (2.2) leads to a different self-energy Σ in the Dyson equation:

$$\Sigma(\varepsilon,\gamma)=1_M\otimes\begin{pmatrix}\Sigma_{ee} & (1-2\gamma)\Sigma_{eh}\\ (1-2\gamma)\Sigma_{he} & \Sigma_{hh}\end{pmatrix}$$
$$=1_M\otimes\frac{\lambda^2}{M}\begin{pmatrix}\langle\mathrm{tr}\,\mathcal{G}_{ee}\rangle & (2\gamma-1)\langle\mathrm{tr}\,\mathcal{G}_{eh}\rangle\\ (2\gamma-1)\langle\mathrm{tr}\,\mathcal{G}_{he}\rangle & \langle\mathrm{tr}\,\mathcal{G}_{hh}\rangle\end{pmatrix}, \tag{A1}$$

where γ is a function of magnetic field [see Eq. (2.3)]. The additional factors of $(1-2\gamma)$ here reflect the fact that breaking time-reversal symmetry suppresses off-diagonal superconducting correlations. Solving the Dyson equation (2.14a) to leading order in $1/M$, we find that relations (2.15a) and (2.15b) continue to hold, meaning that we may still parametrize the self-energies in terms of a pairing angle $\theta(\varepsilon,\gamma)$ through Eq. (2.16a). The equation determining $\theta(\varepsilon,\gamma)$ now takes the form

$$\tan[\theta(\varepsilon,\gamma)]=\frac{N_S Q_S-2\gamma\sin(\theta)}{N_N Q_N-i\pi\varepsilon/2\delta}, \tag{A2}$$

where Q_N and Q_S are functions of θ defined in Eqs. (2.17b) and (2.17c). The $1/M$ corrections to the self-energy in the presence of a magnetic field read

$$\frac{\Sigma_{eh}^2-\Sigma_{ee}^2}{\lambda^2}-1=-\frac{1}{M}\Big(N_S Q_S[\sin(\theta)+Z_S]+N_N Q_N[\cos(\theta)+Z_N]+i\frac{\pi\varepsilon}{2\delta}+2\gamma\sin^2(\theta)\Big). \tag{A3}$$

The next step in the calculation is to sum diagrams for the conductance. The necessary diagrams are the same as those retained in the $B=0$ calculation (i.e., direct and diffusion terms), although their evaluation is different. The direct term is still given by Eq. (2.23a), but with $\theta(\varepsilon,\gamma)$ now determined from Eq. (A2).

The diffusion term acquires a form different from Eq. (2.23b), as factors of $(1-2\gamma)$ now appear in graphs where the particle-hole indices of upper and lower branches do not match. These factors lead to $1/M$ corrections both to the matrix inverse that arises when summing the diffusion ladder, and to the matrix prefactors of the ladder. As discussed earlier, such corrections are important when calculating the conductance. The result is

$$g_{\mathrm{diff}}=8N_N^2\left|\frac{Q_N^2}{Z_N}\right|^2\frac{(1-Z_N^2)^2\tilde{\Lambda}|\sin(\theta)|^2+(\Pi_N+\gamma\Pi_B)|\sin(\theta)|^2+\Pi_S|\cos(\theta)|^2}{\tilde{\Lambda}^2-\tilde{\Omega}^2}, \tag{A4}$$

where

$$\Pi_B(\theta)=2\big((1+Z_N)^2\{1+2\,\mathrm{Re}[\sin^2(\theta)]\}+4Z_N(1+Z_N)\mathrm{Re}[\cos(\theta)]+4Z_N^2\{|\cos(\theta)|^2-2\,\mathrm{Re}[\sin^2(\theta)]\}\big), \tag{A5}$$

$$\tilde{\Lambda}(\theta,\gamma)=\Lambda(\theta)-12\gamma\sin^2(\theta), \tag{A6}$$

$$\tilde{\Omega}(\theta,\gamma)=\Omega(\theta)+4\gamma\{1-|\cos(\theta)|^2+4\,\mathrm{Re}[\sin^2(\theta)]\}\tilde{\Lambda}(\theta,\gamma)+8\gamma\Big(N_N\left|\frac{Q_N}{Z_N}\right|^2Y_N(\theta)+N_S\left|\frac{Q_S}{Z_S}\right|^2Y_S(\theta)+\gamma Y_2(\theta)\Big), \tag{A7}$$

$$Y_N(\theta)=\left(\left|\frac{Z_N}{Q_N}\right|^2-1\right)\{1-|\cos(\theta)|^2+4\,\mathrm{Re}[\sin^2(\theta)]\}-2Z_N\{5\,\mathrm{Re}[\sin^2(\theta)]\mathrm{Re}[\cos(\theta)]+\mathrm{Im}[\sin^2(\theta)]\mathrm{Im}[\cos(\theta)]\}$$
$$+Z_N^2\{1-|\cos(\theta)|^2-2\,\mathrm{Re}[\sin^2(\theta)][1+2|\cos(\theta)|^2]\}, \tag{A8}$$

$$Y_S(\theta)=\left(\left|\frac{Z_N}{Q_N}\right|^2-|1-Z_S\sin(\theta)|^2\right)\{1-|\cos(\theta)|^2+4\,\mathrm{Re}[\sin^2(\theta)]\}-Z_S^2|\sin(\theta)\cos(\theta)|^2, \tag{A9}$$

$$Y_2(\theta)=1-|\cos(\theta)|^2\{1+4\,\mathrm{Re}[\sin(\theta)^2]\}+\mathrm{Re}[3\sin^2(\theta)+4\sin^4(\theta)]+4|\sin(\theta)|^4. \tag{A10}$$

Here $\Lambda(\theta)$, $\Omega(\theta)$, $\Pi_N(\theta)$, and $\Pi_S(\theta)$ are given by Eqs. (2.22a)–(2.22d). The above equations, together with Eq. (A2) for $\theta(\varepsilon,\gamma)$, determine the Andreev conductance for arbitrary voltage and magnetic field.

[1] A. F. Andreev, Zh. Éksp. Teor. Fiz. **46**, 1823 (1964) [Sov. Phys. JETP **19**, 1228 (1964)]; [**49**, 455 (1966)].
[2] C. W. J. Beenakker, Rev. Mod. Phys. **69**, 731 (1997).
[3] I. Kosztin, D. L. Maslov, and P. M. Goldbart, Phys. Rev. Lett. **75**, 1735 (1995).
[4] K. M. Frahm, P. W. Brouwer, J. A. Melsen, and C. W. J. Beenakker, Phys. Rev. Lett. **76**, 2981 (1996).
[5] J. A. Melsen, P. W. Brouwer, K. M. Frahm, and C. W. J. Beenakker, Europhys. Lett. **35**, 7 (1996); Phys. Scr. **T69**, 223 (1997).
[6] A. Altland and M. R. Zirnbauer, Phys. Rev. Lett. **76**, 3420 (1996); Phys. Rev. B **55**, 1142 (1996).
[7] A. Lodder and Yu. V. Nazarov, Phys. Rev. B **58**, 5783 (1998).
[8] P. W. Brouwer and C. W. J. Beenakker, Chaos, Solitons Fractals **7**, 1249 (1997).

[9] H. Schomerus and C. W. J. Beenakker, Phys. Rev. Lett. **82**, 2951 (1999).
[10] W. Ihra, M. Leadbeater, J. L. Vega, and K. Richter, cond-mat/9909100 (unpublished).
[11] N. Argaman, Europhys. Lett. **38**, 231 (1997); N. Argaman and A. Zee, Phys. Rev. B **54**, 7406 (1996).
[12] P. W. Brouwer and C. W. J. Beenakker, J. Math. Phys. **37**, 4904 (1996).
[13] Yu. V. Nazarov and T. H. Stoof, Phys. Rev. Lett. **76**, 823 (1996).
[14] P. Charlat *et al.*, Phys. Rev. Lett. **77**, 4950 (1996).
[15] M. L. Mehta, *Random Matrices* (Academic, New York, 1991).
[16] A. Pandey and M. L. Mehta, Commun. Math. Phys. **87**, 449 (1993).
[17] O. Bohigas, M.-J. Giannonia, A. M. Ozorio de Almeida, and C. Schmit, Nonlinearity **8**, 203 (1995).
[18] K. M. Frahm and J.-L. Pichard, J. Phys. I **5**, 847 (1995).
[19] J. J. M. Verbaarschot, H. A. Weidermuller, and M. R. Zirnbauer, Phys. Rep. **129**, 307 (1985).
[20] Y. Takane and H. Ebisawa, J. Phys. Soc. Jpn. **61**, 1685 (1992).
[21] A. A. Clerk (unpublished).
[22] For a recent review, see W. Belzig, F. K. Wilhelm, C. Bruder, G. Schön, and A. D. Zaikin, Superlattices Microstruct. **25**, 1251 (1999).
[23] Yu. V. Nazarov, Phys. Rev. Lett. **73**, 1420 (1994).
[24] See, e.g., A. D. Stone, in *Physics of Nanostructures*, edited by J. H. Davies and A. R. Long (Institute of Physics, Edinburgh, 1992).
[25] A similar decomposition can be made for transport through a normal dot. In this case, the first term corresponds to direct reflection off tunnel barriers in the contacts, while the second contribution is for processes that explore the dot ergodically. See, e.g., Ref. 2.
[26] G. E. Blonder, M. Tinkham, and T. M. Klapwijk, Phys. Rev. B **25**, 4515 (1982).
[27] B. J. van Wees, P. de Vries, P. Magnée, and T. M. Klapwijk, Phys. Rev. Lett. **69**, 510 (1992).
[28] W. Bauer and G. F. Bertsch, Phys. Rev. Lett. **65**, 2213 (1990).
[29] Note that in the case of a circular dot we make use of wedge-shaped leads for technical convenience. The leads serve both to define scattering modes and to provide boundary conditions for the dot, and thus their particular shape does not affect the conclusions reached here. In the case of wedge-shaped leads, the number of propogating modes in the leads depends on the distance from the center of the circle. We may truncate the number of scattering modes retained because higher order modes (with classical turning points outside the billiard) do not couple to the dot, and thus do not contribute to the Andreev conductance.
[30] H. U. Baranger, R. A. Jalabert, and A. D. Stone, Phys. Rev. Lett. **70**, 3976 (1993); Chaos **3**, 665 (1993).
[31] A. M. Chang, H. U. Baranger, L. N. Pfeiffer, and K. W. West, Phys. Rev. Lett. **73**, 2111 (1994).
[32] J. A. Melsen and C. W. J. Beenakker, Physica B **203**, 213 (1994).
[33] A. F. Volkov, A. V. Zaitsev, and T. M. Klapwijk, Physica C **210**, 21 (1993).
[34] A. F. Morpurgo, S. Holl, B. J. van Wees, and T. M. Klapwijk, Phys. Rev. Lett. **78**, 2636 (1997).
[35] E. Toyoda, H. Takayanagi, and H. Nakano, Physica B **284**, 569 (2000).